Chinese Chemical Letters 34 (2023) 107241

Contents lists available at ScienceDirect

Chinese Chemical Letters

journal homepage: www.elsevier.com/locate/cclet

Amorphous FeCoNi-S as efficient bifunctional electrocatalysts for overall water splitting reaction

Runze He, Chunyan Wang, Ligang Feng*

School of Chemistry and Chemical Engineering, Yangzhou University, Yangzhou 225002, China

ARTICLE INFO

Article history:
Received 20 December 2021
Revised 13 February 2022
Accepted 18 February 2022
Available online 21 February 2022

Keywords:
Bifunctional electrocatalyst
Amorphous
Overall water splitting
FeCoNi hydroxide
Sulfuration

ABSTRACT

Developing bifunctional electrocatalysts for overall water splitting reaction is still highly desired but with large challenges. Herein, an amorphous FeCoNi-S electrocatalyst was developed using thioacetamide for the sulfuration of FeCoNi hydroxide during the hydrothermal process. The obtained catalyst exhibited an amorphous structure with hybrid bonds of metal-S bond and metal-O bonds in the catalyst system. The optimized catalyst showed a largely improved bifunctional catalytic ability to drive water splitting reaction in the alkaline electrolyte compared to the FeCoNi hydroxide. It required an overpotential of 280 mV and 80 mV (No-IR correction) to offer 10 mA/cm^2 for water oxidation and reduction respectively; a low cell voltage of 1.55 V was required to reach 10 mA/cm^2 for the water electrolysis with good stability for 12 h. Moreover, this catalyst system showed high catalytic stability, catalytic kinetics, and Faraday efficiency for water splitting reactions. Considering the very low intrinsic activity of FeCoNi hydroxide, the efficient bifunctional catalytic ability should result from the newly formed hybrid active sites of metallic metal-S species and the high valence state of metal oxide species. This work is effective in the bifunctional catalytic ability boosting for the transition metal materials by facile sulfuration in the hydrothermal approach.

Hydrogen energy plays a very important role for renewable energy sources to replace fossil fuels by compensating their intermittence character [1–3]. The ideal way to produce hydrogen is from the water-splitting technique by making use of sustainable energy. The water splitting has two half-reactions of hydrogen evolution (HER) and oxygen evolution reactions (OER), and the noble metals of Pt, Ir or Ru-based compounds are active catalysts while the potential widespread application is restricted by the high cost and scarcity [4–7]. Common consensus has been made on the development of non-precious transition metal-based catalysts, however, more challenges are still faced on these kinds of catalysts due to their low intrinsic activity [8–10].

Recently, the amorphous materials have been found to possess high catalytic capacity resulting from the short-range ordered but long-range disordered atomic structure [11,12]; the high unsaturated coordination state and surface defects in the amorphous materials could provide many catalytic active centers to accelerate the adsorption of reactants and lower activation energy barriers for the catalysis reactions [13,14]. Among the promising amorphous materials, transition metal-based catalysts of Fe-Co-Ni based oxides [15,16], phosphide compounds [17], hydroxides [18,19] and alloys [20] have been studied for water splitting reactions. For example, amorphous FeCoNi oxide catalysts were reported to have much higher OER performance than that of FeCo/FeNi/NiCo-O or Fe/Co/Ni alone because of the efficient synergistic effect of different types of elements and more catalytic active centers formation during the OER [15]. Meanwhile, the amorphous FeCoNi alloy was also found to have good electrocatalytic performance due to the combined synergistic effect of the three metals and the amorphous structure [20]. The electronic structure modulation of the electrocatalyst by introducing appropriate elements could further increase the catalytic performance due to the unique nano interface and heterojunction formation that can promote more active sites and charge transfer between different components in the electrochemical activation process [21–23]. Sulfuration is a promising strategy to reconstruct the catalyst by increasing the metallic property and generating a more active phase in the catalysis reaction. The increased metallic bonds driven by the sulfur anion would be beneficial to the surface reconstruction of catalytically active species for water splitting reaction [24,25]. Sulfur-doped copper oxide over copper foam exhibited good bifunctional catalytic ability for overall water splitting in the alkaline electrolyte [26]. Enhanced bifunctional catalytic ability catalyzed by 2D Co@S-VMoO$_x$ was also found due to

* Corresponding author.
E-mail address: ligang.feng@yzu.edu.cn (L. Feng).

https://doi.org/10.1016/j.cclet.2022.02.046
1001-8417/

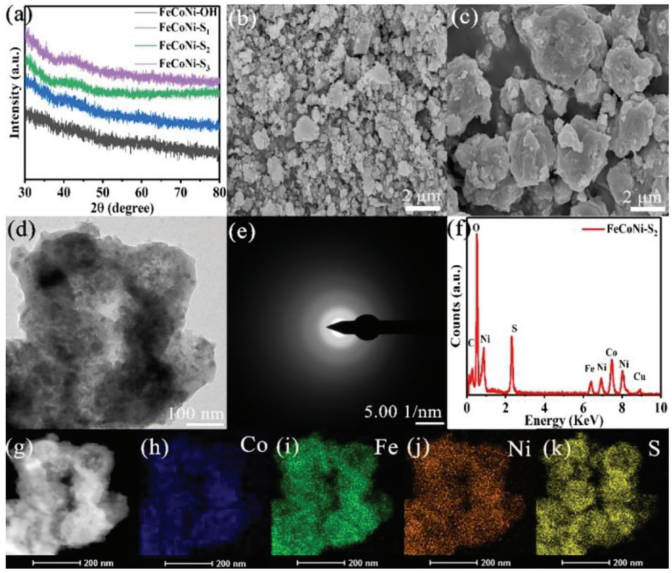

Fig. 1. (a) XRD patterns for FeCoNi-OH, FeCoNi-S_x. SEM image of (b) FeCoNi-OH and (c) FeCoNi-S_2. (d) TEM images, (e) SAED pattern, (f) EDS spectra, STEM image and (g–k) elemental mapping images of FeCoNi-S_2.

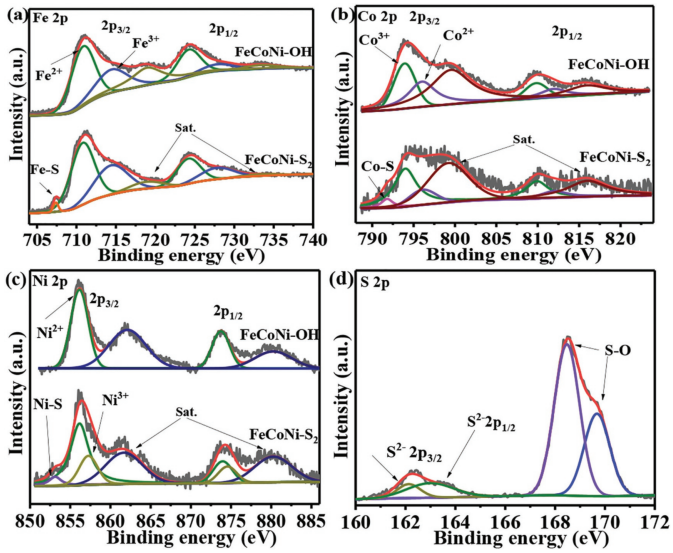

Fig. 2. The high-resolution XPS spectrum of (a) Fe 2p, (b) Co 2p, (c) Ni 2p of FeCoNi-OH and FeCoNi-S_2. The high-resolution XPS spectrum of (d) S 2p of FeCoNi-S_2.

the unusual sulfur doping effect and increased active surface area and conductivity [27].

Considering the above research progress for the non-precious metal catalyst and the necessity of intrinsic activity boosting, herein, we demonstrate the bifunctional catalytic ability for FeCoNi hydroxide (FeCoNi-OH) for water splitting reaction could be largely boosted by the facile mild sulfurization approach using thioacetamide as S source in the hydrothermal synthesis. The sulfurization degree was controlled by the different amounts of thioacetamide during the preparation of the catalysts, and the optimized catalyst showed high catalytic performance for both HER and OER due to the structure reconstruction. An overpotential of 280 mV and 80 mV (No-IR correction) to offer 10 mA/cm^2 for OER and HER was observed and a low cell voltage of 1.55 V was required to reach 10 mA/cm^2 for the water electrolysis when serviced as both anode and cathode catalysts. Considering the very low performance of FeCoNi hydroxide for water splitting reaction, the efficient bifunctional catalytic ability should result from the newly formed hybrid active sites of metallic metal-S species and the high valence state of metal oxide species. The result is instructive for bifunctional catalyst development based on the transition metal materials by facile sulfuration in the hydrothermal approach.

During catalyst fabrication, thioacetamide was employed as the S source to functionalize the FeCoNi hydroxide (FeCoNi-OH), and different amounts of thioacetamide of 112, 224 and 336 mg were added to obtain the corresponding catalysts (FeCoNi-S_x) that were named as FeCoNi-S_1, FeCoNi-S_2 and FeCoNi-S_3. The crystal structure of the FeCoNi-OH and FeCoNi-S_x was probed by powder X-ray diffraction (XRD) technique and there were no obvious diffraction peaks for all the samples, indicating the amorphous or poorly crystallized structure (Fig. 1a). The morphology of these samples was observed by the scanning electron microscope (SEM) technique. Some irregular particles were observed for the FeCoNi-OH sample (Fig. 1b), and the particles became much larger by increasing the content of thioacetamide employed for the sulfur doping (Fig. 1c and Fig. S1 in Supporting information for the rest samples). The local morphology of FeCoNi-S_2, which had the best performance for OER, was further observed by the transmission electron microscopy (TEM) technique (Fig. 1d and Fig. S2 in Supporting information). The large particles were composed of some interconnected small nanoparticles with a diameter of *ca.* 20 nm. No diffraction spots or diffraction rings were observed in the selected area electron diffraction (SAED) pattern, which was consistent with the above amorphous property indicted by the XRD pattern (Fig. 1e). The concerned elements for Fe, Co, Ni and S were found in the energy-dispersive X-ray spectroscopy (EDS) of FeCoNi-S_2 (Fig. 1f), and the atomic ratio of Fe, Co, Ni and S was measured to be 4.60 at%, 5.53 at%, 5.01 at% and 20.30 at%, respectively. The distribution of these elements was shown in the elemental mapping images and they were uniformly distributed over the surface of the sphere particles (Figs. 1g–k).

X-ray photoelectron spectroscopy (XPS) was employed to probe the surface chemical state and the electronic structure. XPS spectrum survey confirmed the presence of concerned elements for FeCoNi-OH and FeCoNi-S_2, and a strong signal of S was observed in the FeCoNi-S_2 (Fig. S3a in Supporting information). The binding energy of the spectrum was calibrated by the C–C bond at 284.8 eV in the C 1s spectrum (Fig. S3b in Supporting information). All the metal elements showed the oxidized state in the FeCoNi-OH precursors, and part of them was transferred to the metal-S bond indicating the successful S incorporation. For the narrow spectrum of the Fe 2p region (Fig. 2a), two bands of $2p_{1/2}$ ad $2p_{3/2}$ were observed that can be deconvoluted into different chemical states and satellite peaks. The peaks at 710.9 and 724.3 eV could be attributed to Fe^{2+}, and those at 714.7 and 728.1 eV were ascribed to Fe^{3+} for the FeCoNi-OH and FeCoNi-S_2 catalysts, along with corresponding satellite portions at 719.4 and 732.8 eV; a peak assigned to the metallic Fe as Fe-S bond in the $2p_{3/2}$ was indicated at 706.8 eV on the FeCoNi-S_2 sample (Table S1 in Supporting information). Due to the formation of the Fe-S bond, the high valent $Fe^{3+}$was also increased in the sample of FeCoNi-S_2 compared to the FeCoNi-OH [28]. The content of Fe^{3+} in FeCoNi-OH was 27.04%, while the content of Fe^{3+} in FeCoNi-S_2 was 35.99%. For the high-resolution spectrum of Co 2p, a fitted peak for the metallic Co as Co-S bond at Co $2p_{3/2}$ was also necessary for the sample of FeCoNi-S_2 (Fig. 2b); the rest peaks assigned to Co^{2+} (796.1 and 812.0 eV), Co^{3+} (794.0 and 809.9 eV) and satellite peaks were found for the Co $2p_{3/2}$ and Co $2p_{1/2}$ in the FeCoNi-OH and FeCoNi-S_2 samples (Table S2 in Supporting information). More content of high valent Co^{3+} was also observed [29,30]. A similar case was also found for the Ni 2p spectrum (Fig. 2c). The metallic state of Ni-S was observed in the Ni

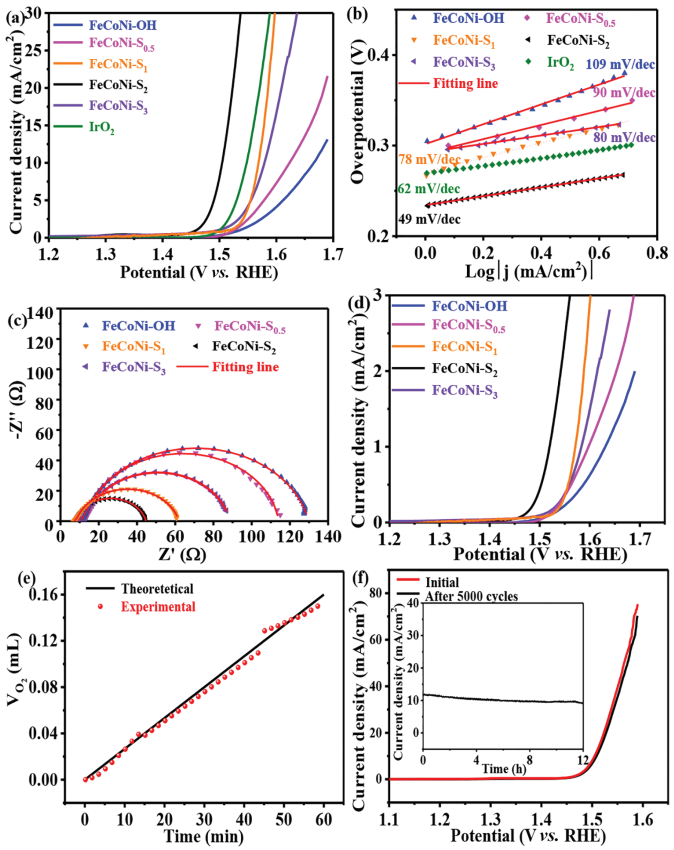

Fig. 3. (a) Polarization curves at 5 mV/s for OER (No-IR correction) and (b) Tafel plots of FeCoNi-OH, FeCoNi-S_x and IrO_2. (c) Nyquist plots at 1.51 V *vs.* RHE, (d) specific activity of FeCoNi-OH and FeCoNi-S_x. (e) Faraday efficiency, (f) polarization curves at 5 mV/s before and after 5000 cycles stability test of FeCoNi-S_2 (inset of chronoamperometry curve at 1.51 V *vs.* RHE for 12 h) of FeCoNi-S_2.

$2p_{3/2}$ at 853.5 eV for FeCoNi-S_2 sample; the characteristic peaks of Ni^{2+} and satellite peaks were observed for the Ni 2p spectrum of FeCoNi-OH sample, while the main peak of Ni 2p was shifted to the high binding energy direction and each band can be deconvoluted into Ni^{2+} and Ni^{3+} for FeCoNi-S_2 catalyst [31,32]. Specifically, the peaks at 856.1 and 873.7 eV could be attributed to Ni^{2+} for the FeCoNi-OH and FeCoNi-S_2 catalysts, and those at 857.0 and 874.6 eV were ascribed to Ni^{3+} for FeCoNi-S_2 catalysts (Table S3 in Supporting information). In the S 2p spectrum of FeCoNi-S_2, the peaks at 163.2 and 162.1 eV belonged to the S^{2-} $2p_{1/2}$ and S^{2-} $2p_{3/2}$ orbitals deriving from the metal-S ligand (Fig. 2d) [33]. Meanwhile, the metal-O bond at 530.1 eV in the O1s spectrum was largely reduced due to the structural transformation to the metal-S bond (Fig. S3c in Supporting information). From the results, it can be seen that sulfurization plays an important role in changing the electronic structure of Co, Ni, and Fe elements, and a partial metal-O bond was transferred to the metal-S bond that can be transferred to a more active phase during the catalysis reaction [34]. Due to the chemical environment change induced by sulfurization, synergism of the metal-O and metal-S bond was realized; the increased metallic state of the metal-S bond and the high valence state of metal species would be beneficial to the following catalysis reaction [35,36].

The above-mentioned catalyst was probed for OER in 1 mol/L KOH electrolyte, and the polarization curves at 5 mV/s for these catalysts were compared (Fig. 3a). To show the performance increase trend, the sample of FeCoNi-$S_{0.5}$ with the thioacetamide amount of 56 mg during the catalyst fabrication was also compared. The electrode of FeCoNi-OH showed a very low performance of ~440 mV overpotentials to reach the current density of 10 mA/cm^2. The catalytic activity was obviously improved when S was added into the catalyst system, and an overpotential of 390 mV was obtained for the FeCoNi-$S_{0.5}$ sample at 10 mA/cm^2. The overpotential to drive this current density was further reduced to 330 mV for FeCoNi-S_1, and the lowest overpotentials of 280 mV were observed on the FeCoNi-S_2 electrode, namely the best catalytic performance for OER. The polarization curves with and without IR-correction of FeCoNi-S_2 catalyst were compared and about 5.0 mV less was required to offer 10 mA/cm^2 (Fig. S4 in Supporting information). The FeCoNi-S_3 electrode showed a reduced performance for OER, and FeCoNi-S_2 even surpassed most of the recently reported FeCoNi-based materials (Table S4 in Supporting information). Furthermore, the catalytic performance of FeCoNi-S_2 was even much better than that of the commercial IrO_2 catalysts (310 mV). The Tafel slope of these catalysts was compared to probe the catalytic mechanism, and the value was 109 and 49 mV/dec for the pristine FeCoNi-OH and FeCoNi-S_2 electrode, respectively (Fig. 3b). The Tafel slope value of 109 mV/dec means the M-O bond formation step as the rate-deterring step catalyzed by FeCoNi-OH, while it was changed to the step of M-O reaction by hydroxyl radical to produce M-OOH as the rate-determining step with the Tafel slope value of 49 mV/dec occurred on the FeCoNi-S_2 electrode [37]. Moreover, FeCoNi-S_2 showed the smallest Tafel slope among all the FeCoNi-S_x samples, indicating its fastest catalytic kinetics [38]. The charge transferability was then probed by the electrochemical impedance spectrum (EIS), and the Nyquist plots of these samples were compared in Fig. 3c. By fitting the Nyquist plot with a typical equivalent circuit (Fig. S5 in Supporting information), the uncompensated solution resistance and the charge transfer resistance were obtained (Table S5 in Supporting information). All the catalysts showed a similar uncompensated solution resistance of *ca.* 8.0 Ω, indicating the similar electrode configuration; FeCoNi-S_2 showed the lowest charge transfer resistance of 37.8 Ω among all the electrodes, indicating the fastest charge transfer ability for OER in the electrode/electrolyte surface.

The catalytic efficiency is a very important factor of a catalyst, and generally, it can be evaluated by the specific activity and the turnover frequency values. To get the specific activity, we firstly measured the electrochemical specific surface area (ECSA) of these catalysts by the double-layer capacitance (C_{dl}) approach used elsewhere [39]. The capacitive current of samples recorded by different scan rates was employed to get the C_{dl} value (Fig. S6 in Supporting information), and the ECSA was calculated by normalizing the C_{dl} (in mF) to the well-recognized reference capacitive of 40 μF/cm^2 for a flat smooth electrode (Table S6 in Supporting information). To be specific, the value for FeCoNi-OH and FeCoNi-S_2 electrode was 0.46 cm^2 and 0.86 cm^2 respectively. The polarization of specific activity was compared by normalizing the current to the ECSA (Fig. 3d). Among all the samples, FeCoNi-S_2 still showed the best catalytic performance, indicating the highest utilization of the active sites. The current density at 1.51 V was 0.74 mA/cm^2 for the FeCoNi-S_2 electrode, about 12 times higher than that of 0.06 mA/cm^2 for the FeCoNi-OH electrode (Table S7 in Supporting information). The high intrinsic activity of the sulfuration catalyst was also verified by the turnover frequency (TOF) polarization curves (Fig. S7 in Supporting information). To be specific, the FeCoNi-S_2 possessed a TOF value of 0.05 s^{-1} at the overpotentials of 280 mV, about 25 times of FeCoNi-OH with the value of 0.002 s^{-1}. Therefore, the largely increased intrinsic activity was realized on the FeCoNi-S_2 compared to the FeCoNi catalyst. It can be seen that the facile S-doping into the FeCoNi during the hydrothermal fabrication not only increased the active site exposure but also boosted the catalytic efficiency of the active sites considering the specific activity and TOF values. The current efficiency of the FeCoNi-S_2 catalyst was evaluated in a gas-tight sealed electro-

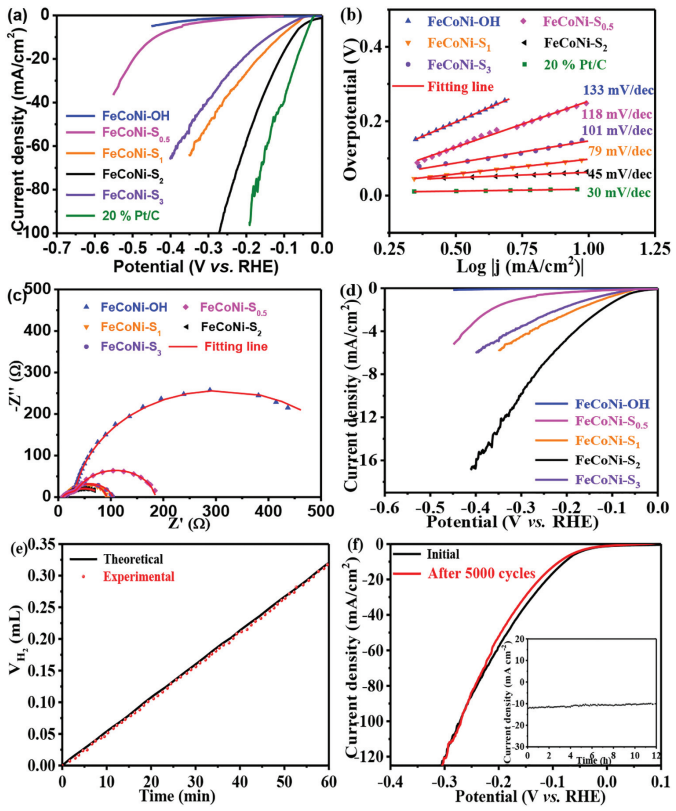

Fig. 4. (a) Polarization curves for HER at 5 mV/s and (b) Tafel plots of FeCoNi-OH, FeCoNi-S_x and 20% Pt/C. (c) Nyquist plots at 0.080 V *vs.* RHE, (d) specific activity of FeCoNi-OH and FeCoNi-S_x. (e) Faraday efficiency, (f) polarization curve at 5 mV/s before and after 5000 CV cycles (inset of chronoamperometry curve at −0.08 V *vs.* RHE for 12 h).

chemical cell, and the amount of the gas was recorded by measuring the gas pressure. By comparing the amount of oxygen produced and the theoretical amount of oxygen generated assuming the faraday efficiency of 100%, the plots of the gas amount collected at the overpotentials of 280 mV for 1 h were quite close to the theoretical result, indicating the current efficiency close to 100% during the catalytic reaction (Fig. 3e). The catalytic stability of the FeCoNi-S_2 catalyst for OER was evaluated by comparing the polarization curve before and after 5000 cycles CV running (Fig. 3f). The polarization curves were overlapped very well where only 5 mV overpotentials increase were found to drive the current density to 10 mA/cm^2. The stability revealed by chronoamperometry measurement was done at 1.51 V for 12 h, and very good stability with very low performance decay was observed (inset of Fig. 3f).

HER is an equally important half-reaction for the overall water splitting reaction, and the HER performance of these catalysts was compared by linear sweep voltammetry (LSV) in the 1 mol/L KOH (Fig. 4a). FeCoNi-OH electrode showed almost no HER activity and the slightly increased performance was found in the FeCoNi-$S_{0.5}$ electrode that required the overpotentials of the 450 mV to reach 10 mA/cm^2. The best catalytic performance was still observed on the FeCoNi-S_2 electrode, which exhibited the smallest overpotential of 80 mV for 10 mA/cm^2 among all the FeCoNi-S_x electrodes. The polarization curves of FeCoNi-S_2 catalysts with and without IR correction were compared, and 8.0 mV less was needed to offer the current density of 10 mA/cm^2 (Fig. S8 in Supporting information). This performance was still lower than that of the commercial Pt/C catalyst (45 mV), while it was still among the TOP catalyst in the family of non-noble catalysts (Table S8 in Supporting information). The Tafel plots of these catalysts were shown in Fig. 4b. A typical value of 30 mV/dec for the Pt/C was observed indicating the Volmer-Tafel step as the rate-determining step. The value for FeCoNi-OH was 133 mV/dec, which follows the mechanism of the Volmer step, and it was transferred to the Volmer–Heyrovsky mechanism for the FeCoNi-S_2 electrode that showed the Tafel slope of *ca.* 45 mV/dec. The largely reduced values of the Tafel slope for FeCoNi-S_2 suggested an increased catalytic kinetic for HER. Following that, the charge transfer resistance was obtained by fitting the Nyquist plots of these samples (Fig. 4c). The R_{ct} of 76.3 Ω was obtained for the FeCoNi-S_2 electrode, much lower than that of other FeCoNi-S_x samples. Compared to the pristine FeCoNi-OH electrode (550 Ω), the advantage of the sulfuration induced charge transfer ability boosting is obvious (Table S9 in Supporting information). Besides, the largely increased intrinsic of the FeCoNi-S_2 electrode for HER was also observed. As compared in the polarization curve of the specific activity (Fig. 4d), FeCoNi-S_2 still showed the highest current density for HER among the samples. A similar result was also found in the TOF curve (Fig. S9 in Supporting information). For example, the specific activity and the TOF value of FeCoNi-S_2 were −0.94 mA/cm^2 and 0.08 s^{-1}, respectively, about 13 times and 40 times of the FeCoNi sample (Table S10 in Supporting information). Faraday efficiency close to 100% for HER was also signified on the FeCoNi-S_2 electrode by comparing theoretically and experimentally obtained hydrogen volume (Fig. 4e). The stability of the FeCoNi-S_2 catalyst for HER was probed by measuring the LSV curve before and after 5000 cycles of voltammetry running (Fig. 4f). Good catalytic stability was also indicated by these polarization curves where very close performance was found. Moreover, the high catalytic stability was also shown in the long-term chronoamperometry measurement (inset of Fig. 4f), where very stable current density during the measurement was observed at −10 mA/cm^2 driven at −0.08 V for 12 h.

It can be seen FeCoNi-OH showed both low performance for HER and OER, but the catalytic ability was largely improved by sulfuration with low S contents due to the improved conductivity and higher polarizability than original oxygen/hydroxide [40,41]. The best one was obtained on the sample of FeCoNi-S_2, and then the performance was reduced if more S was incorporated. The formation of local metal di-sulfide will dilute the metal sits which were adverse to the water dissociation due to the difficulty of surface reconstruction, and anion exchange in the alkaline electrolyte [33,42]. Anyway, the incorporation of S will modify the electronic structure, adsorption energy and reaction pathways, *etc.*, and more studies might be done in future work to probe the details. Since the FeCoNi-S_2 electrode showed high catalytic activity for both HER and OER, the overall water splitting performance was further evaluated using FeCoNi-S_2 as both cathode and anode in a two-electrode water electrolysis system. FeCoNi-S_2 electrode exhibited very attractive performance for water splitting reaction that required a cell voltage of 1.55 V to provide 10 mA/cm^2 on the glass carbon electrode (Fig. 5a). The cell potential was also much lower than that of the commercial system of 20% Pt/C||IrO_2 which needed 1.59 V to reach the same current density. The FeCoNi-OH||FeCoNi-OH required the largest cell voltage of 1.75 V to reach the current density of 10 mA/cm^2, thus the sulfur incorporation induced bi-functional catalytic ability boosting was demonstrated. The stability for water electrolysis revealed by the chronoamperometry test was recorded at 1.55 V for 12 h (Fig. 5b). The current density during the whole test offered by the FeCoNi-S_2 electrode did not change obviously indicating promising catalytic stability for a potential application. On contrary, serious performance decay was observed for the catalyst system of 20% Pt/C||IrO_2 catalyst where *ca.* 70.0% of the initial current density was lost, which was consistent with the reports elsewhere [43]. The FeCoNi-OH||FeCoNi-OH electrode showed the worst catalytic stability, where the current dropped sharply very soon and tended to 0 after 12 h. Be-

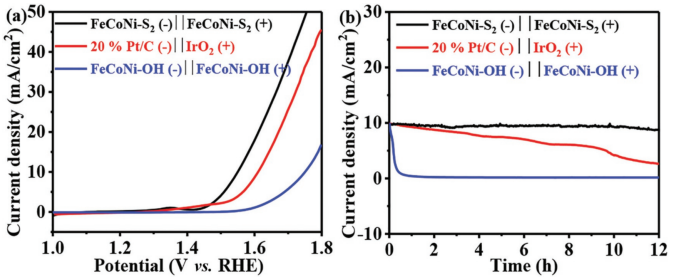

Fig. 5. (a) Polarization curves of FeCoNi-S_2||FeCoNi-S_2, FeCoNi-OH||FeCoNi-OH and 20% Pt/C||IrO_2 for water splitting at 5 mV/s. (b) Chronoamperometry curve of FeCoNi-S_2||FeCoNi-S_2 at 1.55 V, FeCoNi-OH||FeCoNi-OH at 1.75 V and 20% Pt/C||IrO_2 at 1.59 V for 12 h.

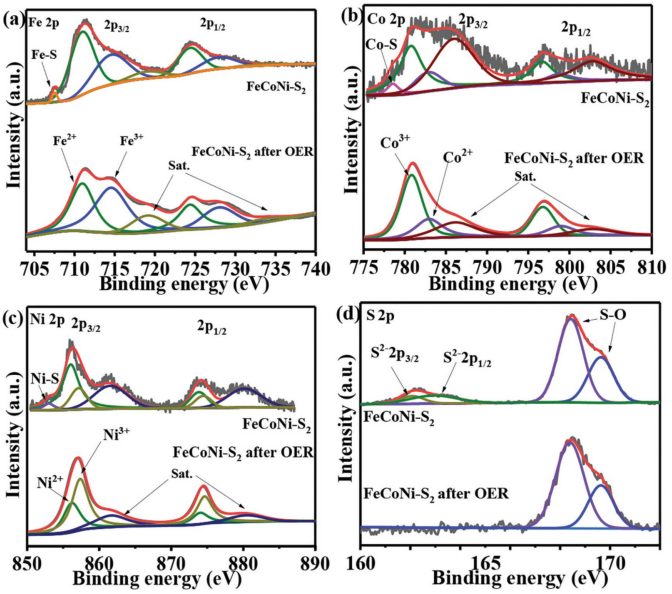

Fig. 6. High-resolution XPS spectra of (a) Fe 2p, (b) Co 2p, (c) Ni 2p and (d) S 2p before and after OER test for FeCoNi-S_2.

sides, the overall water splitting performance offered by FeCoNi-S_2 as bifunctional electrodes was also superior to most of the heterogeneous catalysts (Table S11 in Supporting information). The surface reconstruction for catalysts after long-term water splitting has been largely investigated elsewhere. Generally, there was no obvious modification for the catalyst after HER as it was subjected to a mild reduction condition [44]. Considering the corrosion of the anodic reaction and the structure reconstruction of the catalyst for OER, here, the chemical state change of FeCoNi-S_2 serviced for OER was probed by XPS analysis. For the core-level spectrum of Fe 2p (Fig. 6a), Co 2p (Fig. 6b) and Ni 2p (Fig. 6c), common characters were found for the samples after the OER, where the metal-S bond disappeared and the high valence state of metal species was increased compared to the original sample (Table S12 in Supporting information). To be specific, the ratio of Fe^{3+}/Fe^{2+} was increased from 0.76 to 1.28, and so was Co^{3+}/Co^{2+} (from 2.93 to 4.22), and Ni^{3+}/Ni^{2+} (from 2.37 to 3.57). Meanwhile, the metal-S bond disappeared in the S 2p spectrum due to the surface structure reconstruction from the metallic metal-S bond to the metal-O bond (Fig. 6d). It can be further confirmed by the O 1s spectrum where the metal-oxygen or hydroxide species dominated the main content (Fig. S10 in Supporting information). This high valence state metal species formation was driven by the high oxidation potentials for OER, and this phenomenon was generally observed for the transition metal pre-catalysts like metal nitride, fluoride, sulfide, or phosphide [45]. Considering the low performance of the FeCoNi-OH for the water-splitting reaction, the mixed bonds of metal-O and metal-S formation might offer the bifunctional active sites for the overall water splitting, namely, the metal-S bond contributed to the HER and the high valence state of metal-O bond service for the OER.

In conclusion, an amorphous FeCoNi-S catalyst was demonstrated effective as a bifunctional catalyst in the overall water splitting reaction. The catalyst can be easily prepared using thioacetamide as S source during the hydrothermal process, and the amount of thioacetamide largely influenced the catalytic performance. The obtained catalyst showed an amorphous structure and the hybrid bonds of metal-S bond and metal-O were indicated in the system. FeCoNi-S_2 showed the best catalytic performance for OER and HER among all the catalysts, with the overpotentials of 280 and 80 mV to drive 10 mA/cm^2 respectively, much smaller than that of the control sample of FeCoNi-OH. In light of the bifunctional catalytic ability, a low cell voltage of 1.55 V was required to provide 10 mA/cm^2. Moreover, high catalytic stability, catalytic kinetics, and Faraday efficiency were demonstrated for this system. The efficient bifunctional catalytic ability could result from the metallic metal-S species for HER and the high valence state of metal oxide species for the OER. This work showed an effective approach to trigger the bifunctional catalytic ability of transition metal materials by facile sulfuration in the hydrothermal approach.

Declaration of competing interest

The authors declare that they have no known competing financial interests or personal relationships that could have appeared to influence the work reported in this paper.

Acknowledgments

The work is supported by the National Natural Science Foundation of China (No. 21972124) and the Priority Academic Program Development of Jiangsu Higher Education Institution. L. Feng appreciated the support of the Six Talent Peaks Project of Jiangsu Province (No. XCL-070–2018).

Supplementary materials

Supplementary material associated with this article can be found, in the online version, at doi:10.1016/j.cclet.2022.02.046.

References

[1] P. Han, T. Tan, F. Wu, et al., Chin. Chem. Lett. 31 (2020) 2469–2472.
[2] Y. Zhou, D. Liu, W. Qiao, et al., Mater. Today Phys. 17 (2021) 100357.
[3] B. Fang, L. Feng, Acta Phys. Chim. Sin. 36 (2020) 1905023.
[4] R. He, M. Li, W. Qiao, et al., Chem. Eng. J. 423 (2021) 130168.
[5] L. Yang, Z. Liu, S. Zhu, et al., Mater. Today Phys. 16 (2021) 100292.
[6] L. Chen, Y. Wang, X. Zhao, et al., J. Mater. Sci. Technol. 110 (2022) 128–135.
[7] Y. Bao, M. Zha, P. Sun, et al., J. Energy Chem. 59 (2021) 748–754.
[8] X. Li, C. Huang, W. Han, et al., Chin. Chem. Lett. 32 (2021) 2597–2616.
[9] D. Li, H. Liu, L. Feng, Energy Fuels 34 (2020) 13491–13522.
[10] S. Xu, Y. Du, X. Yu, et al., Nanoscale 13 (2021) 17003–17010.
[11] J. Liu, J. Nai, T. You, et al., Small 14 (2018) 1703514.
[12] Z. Jin, P. Li, X. Huang, et al., J. Mater. Chem. A 2 (2014) 18593–18599.
[13] T. Kou, S. Wang, J.L. Hauser, et al., ACS Energy Lett. 4 (2019) 622–628.
[14] D. Ding, J. Huang, X. Deng, et al., Energy Fuels 35 (2021) 15472–15488.
[15] L. Bai, X. Wen, J. Guan, Mater. Today Energy 12 (2019) 311–317.
[16] M. Zha, C. Pei, Q. Wang, et al., J. Energy Chem. 47 (2020) 166–171.
[17] R. Yao, Y. Wu, M. Wang, et al., Int. J. Hydrog. Energy 44 (2019) 30196–30207.
[18] R. Fan, Y. Zhou, M. Li, et al., Chem. Eng. J. 426 (2021) 131943.
[19] Y. Zhou, F. Wang, S. Dou, et al., Chem. Eng. J. 427 (2022) 131643.
[20] S. Saha, A.K. Ganguli, ChemistrySelect 2 (2017) 1630–1636.
[21] M. Al-Mamun, Z. Zhu, H. Yin, et al., Chem. Commun. 52 (2016) 9450–9453.
[22] X. Gu, Z. Liu, M. Li, et al., Appl. Catal. B: Environ. 297 (2021) 120462.
[23] J. Li, S. Wang, J. Chang, et al., Adv. Powder Mater. 1 (2022) 100030.
[24] Y. Zhou, W. Yu, Y. Cao, et al., Appl. Catal. B 292 (2021) 120150.
[25] K. Wan, J. Luo, X. Zhang, et al., J. Energy Chem. 62 (2021) 198–203.
[26] X. Zhang, X. Cui, Y. Sun, et al., ACS Appl. Mater. Interfaces 10 (2018) 745–752.

[27] J. Wang, D.T. Tran, K. Chang, et al., ACS Appl. Mater. Interfaces 13 (2021) 42944–42956.
[28] Z. Li, X. Wu, X. Jiang, et al., Adv. Powder Mater. 33 (2022) 1105–1109.
[29] D.Y. Li, L.L. Liao, H.Q. Zhou, et al., Mater. Today Phys. 16 (2021) 100314.
[30] S. Wang, L. Zhao, J. Li, et al., J. Energy Chem. 66 (2022) 483–492.
[31] B. Fang, Z. Liu, Y. Bao, et al., Chin. Chem. Lett. 31 (2020) 2259–2262.
[32] S. Wang, J. Zhu, X. Wu, et al., Chin. Chem. Lett. 33 (2022) 1105–1109.
[33] H. Liu, Z. Liu, F. Wang, et al., Chem. Eng. J. 397 (2020) 125507.
[34] G. Hai, H. Gao, G. Zhao, et al., iScience 20 (2019) 481–488.
[35] H. Liu, S. Cao, J. Zhang, et al., Mater. Today Phys. 20 (2021) 100448.
[36] B. Zhang, L. Wang, Z. Cao, et al., Nat. Catal. 3 (2020) 985–992.
[37] N. Suen, S. Hung, Q. Quan, et al., Chem. Soc. Rev. 46 (2017) 337–365.
[38] Y. Bao, L. Feng, Acta Phys. Chim. Sin. 37 (2021) 2008031.
[39] M. Li, Y. Gu, Y. Chang, et al., Chem. Eng. J. 425 (2021) 130686.
[40] H. Wang, C. Tang, B. Wang, et al., Adv. Mater. 29 (2017) 1702327.
[41] B. Li, S. Zhang, C. Tang, et al., Small 13 (2017) 1700610.
[42] L. Yang, M. Gao, B. Dai, et al., Electrochim. Acta 191 (2016) 813–820.
[43] G. Zhang, B. Wang, L. Li, et al., Small 15 (2019) 1904105.
[44] Y. Lu, Z. Li, Y. Xu, et al., Chem. Eng. J. 411 (2021) 128433.
[45] Z. Liu, H. Liu, X. Gu, et al., Chem. Eng. J. 397 (2020) 125500.